THEORY OF LONGITUDINAL BEAM HALO IN RF LINACS: II. ENVELOPE-PARTICLE RESONANCES*

Steven M. Lund and John J. Barnard
Lawrence Livermore National Laboratory, L-440, Livermore, CA 94550

Abstract

Using the core/test-particle model described in a companion paper in these proceedings[1] ("Theory of Longitudinal Halo in rf Linacs: I. Core/Test-Particle Formulation," by J. J. Barnard and S. M. Lund), we analyze longitudinal beam halo produced by resonant self-field interactions in intense, ion-beam rf linacs. It is shown that particles moving in the presence of the space-charge forces of an oscillating, mismatched ellipsoidal beam bunch can be resonantly driven to large longitudinal amplitude. This resonantly produced halo is first analyzed in a limit where it is most simply understood, with particles moving purely longitudinally and with linear rf focusing. Then modifications of the resonance induced by nonlinear rf and transverse-longitudinal coupling are explored.

1 INTRODUCTION

Resonant interactions between particle orbits and oscillating space-charge forces associated with a mismatched beam core are known to be a significant cause of transverse ($\perp$) beam halo[I2−I5,2−4]. Recently, simulation work using idealized core/test-particle models has suggested that analogous, resonantly produced halo may occur longitudinally and be an issue of concern in intense-beam applications[2]. Here, we examine resonantly produced longitudinal ($\parallel$) halo using a more detailed core/test-particle model developed in an accompanying paper (Ref. 1, hereafter referred to as Paper I). In Paper I it was shown that a low-frequency mode (LFM) of a mismatched ellipsoidal beam bunch with uniform space-charge can drive a low-order longitudinal resonance (LR). This LR leads to $\parallel$ beam halo with analogous properties to that of resonantly produced $\perp$ halo[I2−I5]. To understand the essential physics that determines the structure of the resulting $\parallel$ halo, the LR is numerically and analytically analyzed under increasingly realistic conditions in Secs. II-IV. The notation employed in this paper is developed in Paper I. Specific references to citations and equations from Paper I will be denoted by the prefix I. All model results are illustrated using the parameters of the 100 MeV point of an intense proton-beam linac presented in the Table of Paper I. This linac is the normal conducting design originally considered for the Accelerator Production of Tritium (APT) project.

2 LINEAR RF FOCUSING

To simply elucidate the essential features of the LR, a linear rf approximation is taken [see Eq. (I-5)] where the $\parallel$ focusing force is linear about displacements from the synchronous particle, envelope motion is assumed to be in a pure linear LFM (as opposed to a general linear mode superposition of a LFM and HFM, or a finite amplitude solution to the full nonlinear envelope equations), and only on-axis particles (i.e., $\mathbf{x}_\perp = 0$) are considered. To visualize the structure of the LR in $\Delta\phi - \Delta\mathcal{E}$ phase-space, particles are initialized with $\Delta\mathcal{E} = 0$ and $\Delta\phi$ uniformly distributed over half the phase-width of the rf bucket and Poincaré plot images of the particle phase-space are formed by numerically integrating Eqs. (I-4) with respect to s and superimposing strobed snapshots of the $\parallel$ phase-space accumulated at s where the $\parallel$ envelope radius r_z is minimum (at s-increments of $2\pi/k_L$). A typical Poincaré plot produced by accumulating long enough to clearly visualize the LR is presented in Fig. 1(a) for 20 particles and an envelope mode amplitude of $\delta r_z/r_{z0} = 0.1$. The solid vertical lines indicate the phase width of the equilibrium beam radius r_{z0} and the dashed vertical lines indicate the phase extent of the envelope oscillations. Particles deep within and far outside the core of the beam undergo simple depressed and undepressed synchrotron oscillations, respectively. At intermediate particle oscillation amplitudes there is a strongly expressed resonant structure in which particles

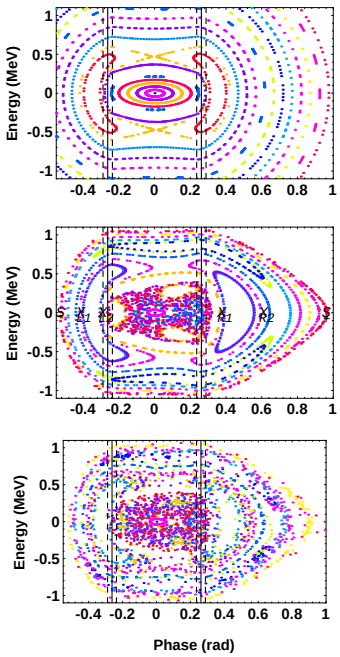

Figure 1: Poincaré plots of energy ($\Delta\mathcal{E}$) and phase ($\Delta\phi$) phase-space for $\delta r_z/r_{z0} = 0.1$, $I = 200$ mA, and: **a.** (top) Linear rf and $\mathbf{x}_\perp = 0$. **b.** (middle) Nonlinear rf and $\mathbf{x}_\perp = 0$. **c.** (bottom) Nonlinear rf and $\mathbf{x}_\perp \neq 0$.

* Work performed under the auspices of the U.S. D.O.E. by LLNL under contract W-7405-ENG-48

0-7803-4376-X/98/$10.00 © 1998 IEEE

undergo approximately two oscillation periods over a LFM envelope period, thereby identifying the LR suggested in Paper I. Higher-order resonances with smaller particle oscillation amplitudes also appear. Such resonances become stronger and interact with the LR with increasing space-charge forces (i.e., increasing I).

In analogy to Gluckstern's analysis of transverse beam halo[I4], the LR can be analyzed analytically if, in addition to the assumptions above, a limit of a spherical bunch in the beam frame (i.e., $\gamma_s r_{z0} = r_{\perp 0}$) is taken. In this case, the space-charge force exterior to the bunch [see Eq. (I-1)] has a simple inverse-square fall-off $\sim \Delta z/|\Delta z|^3$ exterior to the bunch, and the equations of motion (I-4) can be expressed in a phase-amplitude form and with all non-resonant phases averaged over to derive a phase-averaged constant of the motion[I7]. This constant can be interpreted as a resonant particle Hamiltonian given by (1)

$$H = -(2k_s - k_L)w - \frac{k_{sc}^2}{\pi k_s}\left\{(w-6)\left[\pi - 2\sin^{-1}\left(\frac{1}{\sqrt{w}}\right)\right] + 2\sqrt{w-1} + \frac{8}{\sqrt{w}}\ln\left(\sqrt{w}+\sqrt{w-1}\right)\right\}\Theta(w-1) - \frac{3k_{sc}^2}{k_s}\left(\frac{\delta r_z}{r_{z0}}\right)\left\{\frac{1}{2} + \frac{1}{\pi}\left[\sin^{-1}\left(\frac{1}{\sqrt{w}}\right) - \frac{\pi}{2} - \frac{\sqrt{w-1}(w-2)}{w^2}\right]\Theta(w-1)\right\} w\cos\Psi,$$

where $k_{sc} = \sqrt{K_{3D}/3\gamma_s^2 r_{z0}^3}$ is a space-charge wavenumber, $\Theta(w-1)$ is a Θ-function with $\Theta(w-1) = 1$ for $w > 1$ and $\Theta(w-1) = 0$ for $w < 1$, and (w, Ψ) are coordinates related to the $(\Delta\phi, \Delta\mathcal{E})$ coordinates as

$$w = \left(\frac{\Delta\mathcal{E}}{\Delta\mathcal{E}_b}\right)^2 + \left(\frac{\Delta\phi}{\Delta\phi_b}\right)^2, \qquad (2)$$

$$w\cos\Psi = \left(\frac{\Delta\mathcal{E}^2}{\Delta\mathcal{E}_b^2} - \frac{\Delta\phi^2}{\Delta\phi_b^2}\right)\cos k_L s - 2\frac{\Delta\phi}{\Delta\phi_b}\frac{\Delta\mathcal{E}}{\Delta\mathcal{E}_b}\sin k_L s.$$

Here, $\Delta\phi_b \equiv 2\pi r_{z0}/\beta_s\lambda$ and $\Delta\mathcal{E}_b \equiv mc^2\gamma_s^3\beta_s^2 k_s r_{z0}$ are the equilibrium bunch radii in phase and energy, and envelope oscillations with $r_z = r_{z0} - \delta r_z\cos(k_L s)$ are assumed. The LR phase-space determined by the $H = $ const. surfaces of this *spherical* bunch conservation constraint is plotted in Fig. 2 for $I = 50$ mA (other parameters fixed) and with the characteristic frequencies k_s, k_{sc} and k_L, equilibrium radius r_{z0}, and mode amplitude $\delta r_z/r_{z0}$ taken from the *ellipsoidal* bunch problem. The corresponding numerically calculated Poincaré plot of the ellipsoidal bunch is shown in overlay. The rough agreement between these solutions is due to an insensitivity of the LR structure with respect to the precise nature of the $\|$ space-charge force. For example, if the inverse-square fall-off in the exterior space-charge force law is replaced by one with a more rapid falloff, similar conservation constraints can be derived and little change is observed in the LR structure. However, this agreement appears to break down at higher bunch currents I, suggesting a limit to this argument that has yet to be quantified in detail.

3 NON-LINEAR RF FOCUSING

The linear rf approximation fails as distance from the synchronous particle is increased. Moreover, even the equilibrium bunch can occupy a significant fraction of the rf

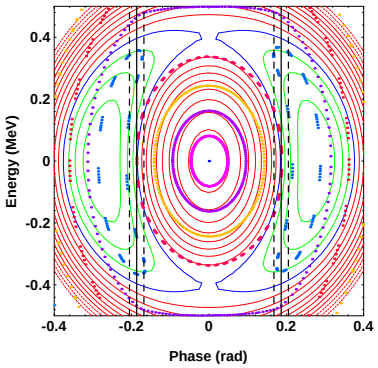

Figure 2: Overlay of theoretical (spherical bunch) and simulated (elliptical bunch) LR energy ($\Delta\mathcal{E}$) and phase ($\Delta\phi$) phase-space for linear rf, $\mathbf{x}_\perp = 0$, $I = 50$ mA.

wavelength. In this section, modifications of the LR induced by the sinusoidal nature of the applied rf focusing are analyzed numerically. For simplicity, all assumptions outside of the linear rf focusing limit of the ellipsoidal beam analysis in Sec. II are maintained (i.e., on-axis particles and a linear LFM envelope mode). The phase space obtained is presented in Fig. 1(b) for the same parameters as Fig. 1(a). Note that the LR structure now has a left-right asymmetry associated with the anharmonic nature of the rf focusing and is well confined within the separatrix of particle loss for the rf bucket. At larger mismatch amplitudes $\delta r_z/r_{z0}$ the structure becomes broader and moves closer to bucket seperatrix, but for $|\delta r_z|/r_{z0} < 0.5$ does not lead to particle loss from the bucket. This result is illustrated in Fig. 3, where the phase-variation (in $\Delta\phi$) of labeled structure features is plotted as a function of mismatch amplitude $|\delta r_z|/r_{z0}$. Note that the width of the LR structure (as measured by the phase widths of X_{L1} to X_{L2} and X_{R1} to X_{R2}) increases with amplitude and approaches the beam core, while the structure O-point varies little with amplitude. At large amplitudes, the close proximity of the LR structure to the core ($\pm\Delta\phi_{eq}$ = phase edges of core) suggests that it will be easily populated, potentially degrading beam quality. However, as a consequence of the nonlinear field structure, halo extent appears to remain confined within the extent of the rf bucket (indicated with $S_\pm$ markers).

When the bunch current I is varied with nonlinear rf focusing, an interesting bifurcation of the LR is observed. Namely, at low- ($I < 22.1$ mA) and high-currents ($I > 284$ mA), the low-order LR disappears. Furthermore, at high-currents, higher-order resonances with smaller particle oscillation amplitude appear to dominate. This situation can be understood with reference to Fig. 4. Here, the maximum particle frequency k_M, which generally occurs exterior to the beam core, is numerically calculated as a function of I (with other parameters fixed). Note that for low and high currents, half the LFM frequency ($k_L/2$) falls above the maximum frequency k_M, thereby precluding the LR (see arguments in Paper I). Note that higher-order resonances are still possible for $I > 283$ mA as demonstrated by the

$k_L/3$ curve falling between k_M and the depressed core frequency k_s. Consistent with Fig. 4, no resonances are observed for $I < 22.1$ mA.

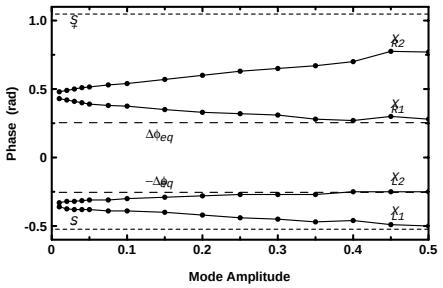

Figure 3: Phase ($\Delta\phi$) measures of LR features versus mode amplitude ($|\delta r_z|/r_{z0}$) for nonlinear rf, $\mathbf{x}_\perp = 0$, $I = 200$ mA.

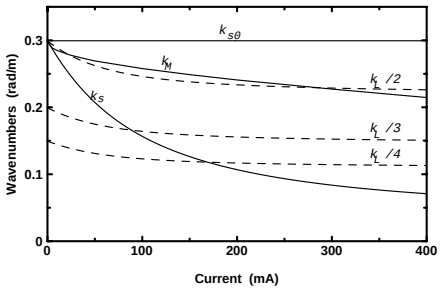

Figure 4: Maximum particle (k_M), depressed and undepressed synchrotron (k_s and k_{s0}), and subharmonic LFM envelope mode ($k_L/2$, $k_L/3$, and $k_L/4$) frequencies versus bunch current I with nonlinear rf.

4 EFFECTS OF $\perp$ / $\parallel$ COUPLING

Since the accelerator beams have finite $\perp$ emittance, particles will, in general, have finite $\perp$ betatron oscillations ($\mathbf{x}_\perp \neq 0$) and, outside the bunch, this motion will introduce $\perp/\parallel$ coupling in the particle equations of motion. This coupling is included in the core/
test-particle model derived in Paper I. In this section, we analyze the effects of this $\perp/\parallel$ coupling on the LR. In Fig. 1(c), we show a Poincaré phase space plot for the same parameters as Fig. 1(b), with the exception that all particles are initialized at $x = 0.6r_{\perp 0}$ instead of $\mathbf{x}_\perp = 0$. Notice that the LR structure persists, although it is somewhat smeared.

It has been noted[3] that under some circumstances $\parallel$ particle oscillation amplitude can be converted into larger $\perp$ oscillation amplitude. We confirm the qualitative observation that such conversion occurs, but fail to confirm the magnitude of the effect. To investigate this we simulated four particles, all with identical initial $\perp$ coordinates $x = 0.6r_{\perp 0} = 1.1$ mm and varying initial $\parallel$ Δz (three with $\Delta z/r_{z0}$ = 0.4, 0.94, and 2.5, and a fourth at 0.80 of the maximum $\parallel$ phase of the stable rf bucket at $\Delta z/r_{z0} = 3.0$). These scaled parameters were similar to those employed in Ref. 3, although the overall beam and accelerator parameters were different. As in Ref. 3, we initialized the LFM and HFM envelope mismatch modes consistent with total amplitudes of $\delta r_z/r_{z0} = 0.1$ and $\delta r_\perp/r_{\perp 0} = 0.1$, and numerically integrated the equations of motion (I-4) for the four particles under the approximation of linear rf focusing. In Fig. 5 we present a Poincaré plot of the transverse ($x - x'$) phase-space obtained while strobing at the frequency of the HFM. The two particles with the large initial $\parallel$ amplitudes increased their $\perp$ amplitudes by a factor of approximately 1.8, reaching amplitudes slightly exterior to the $\perp$ beam extent. This is in contrast to factors of up to 30 seen in Ref. 3. For these parameters, a factor of 1.8 is consistent with particle motion bounded by the equipotential corresponding to the total energy of a particle moving in the potential well of a *matched* beam[I7]. The main effect of the coupling appears to allow the particles to access a larger fraction of the available phase-space bounded by the total potential in the absence of mismatch.

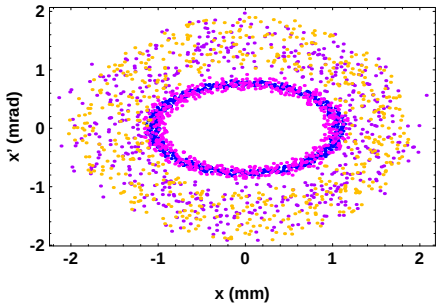

Figure 5: Poincaré plot of $\perp$ phase-space of four particles with identical initial $x = 0.6r_{\perp 0} = 1.1$ mm and varying initial Δz interior and exterior to the core.

5 CONCLUSIONS

A core/test-particle model developed in Ref. 1 has been employed to explore $\parallel$ beam halo due to resonant interactions with envelope oscillations. Characteristic frequencies of particle and envelope oscillations play a critical role in determining the extent and structure of the halo. Model predictions of halo extent are shown to persist under increasingly realistic conditions.

6 ACKNOWLEDGMENTS

The authors wish to again thank R. Ryne, T. Wangler, and R. Gluckstern and in addition note helpful discussions with D. Bruhwiler ($\perp$ / $\parallel$ coupling) and C. Chen, A. Friedman, and I. Hofmann.

7 REFERENCES

[1] J.J. Barnard and S.M. Lund, "Theory of Longitudinal Beam Halo in RF Linacs: I. Core/Test-Particle Formulation," these proceedings.

[2] T.P. Wangler, R.W. Garnett, E.R. Gray, R.D. Ryne, and T.S. Wang, Proc. of the XVIII Int. Linear Accel. Conf., Geneva, 1996, p. 372.

[3] D.L. Bruhwiler, loc. cit. 2.

[4] M. Pabst and K. Bongardt, loc. cit. 2.